Microstructural Effects on Fracture Toughness in AA7010 Plate

B. MORERE, J.-C. EHRSTRÖM, P.J. GREGSON, and I. SINCLAIR

The influence of recrystallization and quench rate after solution treatment on the fracture toughness of 7010 aluminum plate has been studied in longitudinal-transverse (L-T) and short-longitudinal (S-L) orientations for T76-type heat treatments. Extensive fractographic analysis was carried out to identify the failure mechanisms, including simultaneous scanning electron microscope (SEM) observation of fracture surfaces and underlying microstructures. A slow quench rate was strongly detrimental because it modified the dominant failure mode from a relatively high energy primary void growth mechanism to lower energy transgranular shear and grain boundary ductile failure in the L-T and S-L orientations, respectively. Low energy failure was associated with coarse η precipitation during the quench in both L-T and S-L orientation tests, with intragranular and intersubgranular particles contributing to L-T quench sensitivity, and intergranular particles contributing to S-L sensitivity. Partial recrystallization was generally detrimental, with recrystallized grains being shown to be a preferential crack path. The commonly supposed susceptibility of recrystallized grains to intergranular failure did not explain this behavior, particularly in fast quench materials, as recrystallized grains primarily failed by transgranular void growth from the large intermetallics with which they were intrinsically associated. Exceptional S-L orientation quench sensitivity was observed in unrecrystallized material and attributed to a synergistic interaction between heterogeneous boundary precipitation and the specific location of coarse intermetallics along grain boundaries in the unrecrystallized condition. Quantitative assessment of individual contributions to overall fracture resistance is discussed for cases where multiple failure mechanisms occur, highlighting the importance of interacting and noninteracting mechanisms.

I. INTRODUCTION

THE fracture toughness of high strength aluminum alloys is known to depend on many parameters, including flow strength, work hardening rate, slip character, dispersoid content, intermetallic content, grain structure, and grain boundary structure.[1] Furthermore, microstructural anisotropy associated with wrought materials may influence failure mode depending on load and crack orientation. Various models have been put forward in the literature to predict the influence of microstructural or mechanical parameters on the fracture toughness. Following from Hahn and Rosenfield's[2] and Rice and Johnson's[3] work, where unstable crack extension is assumed to proceed when crack tip opening (characterizing the extent of the highly strained region ahead of the crack) reaches the length of the unbroken ligaments separating cracked inclusions, the following expression may be derived:

$$K_{IC} \approx \left[2\sigma_y E \left(\frac{\pi}{6} \right)^{1/3} D \right]^{1/2} f_v^{-1/6} \qquad [1]$$

where D is the diameter of the large inclusions; f_v is their volume fraction; σ_y and E are the yield stress and Young's modulus, respectively; and K_{IC} is the plane strain fracture toughness. This model has been shown to give a reasonable prediction of the effect of the volume fraction of inclusions for constant yield strength and constant particle size in a number of systems, but does not agree with experimental results concerning the influence of yield stress. In an earlier model, Hahn and Rosenfield[4] considered the effects of strain hardening coefficient and yield stress on toughness, particularly in terms of the increased flow localization, and hence crack tip "damage," that occurs with decreasing work-hardening rate. Garrett and Knott[5] reviewed the derivation of this model leading to the relationship

$$K_{IC} \approx \sqrt{\frac{2CE\varepsilon_c^* \sigma_y n^2}{1 - \nu^2}} \qquad [2]$$

where C is a constant, ε_c* is the critical crack tip strain at which unstable propagation occurs, n is the work hardening exponent, and ν is the Poisson ratio. The term ε_c* is taken to be a function of the volume fraction of void nucleating particles.[6] The predicted $n\sqrt{\sigma_y}$ dependency of the fracture toughness for a constant distribution of particles has been shown to provide a reasonable description of toughness behavior as a function of aging between under- and overaged conditions (*i.e.*, varying yield strength) for several Al-based alloys.

Chen and Knott[7] have studied the effect of grain refining dispersoid particles on the toughness of 7xxx-series alloys, indicating that strain localization within shear bands in the plastic zone ahead of the crack tip could lead to decohesion of the interface between the matrix and dispersoids. Fast shear coalescence of the primary voids then occurred *via* the bands, with fracture surfaces exhibiting characteristic fine void sheets. They proposed the use of a critical stress criterion to describe the decohesion of the interface between

B. MORERE and J.-C. EHRSTRÖM, Research Scientists, are with Pechiney CRV, Voreppe, France 38340. P.J. GREGSON, Professor of Aerospace Materials, and I. SINCLAIR, Lecturer, are with the Department of Engineering Materials, University of Southampton, Southampton, SO17 1BJ, United Kingdom.

Manuscript submitted August 17, 1998.

the matrix and the dispersoids. By using the same description of the plastic zone as Hahn and Rosenfield in the preceding model, the following relationship is derived:

$$K_{IC} = \sqrt{CE\sigma_c\sigma_y n^2 \frac{\lambda}{d}} \qquad [3]$$

where σ_c is the critical dispersoid-matrix decohesion stress, λ is the dispersoid spacing, and d is the dispersoid diameter.

The preceding models are related to transgranular ductile failure. However, fracture in high strength aluminum alloys can also proceed by a ductile intergranular mechanism, depending primarily on the aging conditions.[8–14,27,28] Vasudevan and Doherty[8] have reviewed the parameters that promote grain boundary ductile failure, indicating the primary roles of void initiation at boundary precipitates, strain localization within soft precipitate free zones (PFZs), and "planar" deformation within the grain bulk promoting stress/strain concentration at slip band/grain boundary intersections. Gräf and Hornbogen[9] have, for example, modified Hahn and Rosenfield's initial model to take into account the microscopic strain inhomogeneities associated with grain boundary PFZ, assuming that plastic deformation is entirely restricted to the PFZ region, *i.e.*, PFZ flow stress is very much smaller than within the grains, which should be most representative of peak-aged materials. The critical strain at which crack propagation occurs, $\varepsilon_{c\mathrm{PFZ}}$, is now dependent on the grain boundary particles, with K_{IC} taking the form

$$K_{IC} = \sqrt{CE\varepsilon_{c\mathrm{PFZ}}\ \sigma_{\mathrm{PFZ}} n_{\mathrm{PFZ}}^2 \frac{d_{\mathrm{PFZ}}}{D_{\mathrm{grain}}}} \qquad [4]$$

where C is a constant, σ_{PFZ} the PFZ flow stress, d_{PFZ} the PFZ width, and D_{grain} the overall grain size.

Overall, it is recognized that varying microstructural conditions may favor quite different combinations of failure modes in high strength aluminum materials, with the preceding simplified approaches then being applicable individually or in combination in different cases. In the present fracture study, the influences of, and synergy between, thermomechanical processing and quench rate after solution treatment have been considered. The former modifies grain structure, while the latter primarily affects the state of precipitation within the matrix and at grain boundaries. Previous authors have considered their influence on fracture toughness,[11–14] concluding that increased recrystallization levels and/or slow quench rates primarily compromise fracture resistance by promoting grain boundary failure. However, detailed and systematic fractographic studies of crack/microstructure interactions and associated toughness implications in realistic commercial microstructures have not been widely reported. In the present work, quench rate and recrystallization effects have been particularly studied for constant yield strength levels (to ensure comparability of results) in AA7010-T76 plate as a function of underlying material anisotropy (*i.e.*, varying test orientation) at relatively low recrystallization levels representative of commercial thick plate product forms.

II. EXPERIMENTAL PROCEDURE

A. *Material and Characterization*

Four different microstructural states were studied: unrecrystallized/slow quench (USQ), unrecrystallized/fast quench (UFQ), partially recrystallized/slow quench (PRSQ), and partially recrystallized/fast quench (PRFQ). Two commercial AA7010 plates (60-mm gage) were supplied by Pechiney CRV: one in a standard commercial hot-rolled condition giving an unrecrystallized structure, and the other additionally hot rolled at ~350 °C to produce partial recrystallization (Table I for compositions). After solution treatment (2 hours at 472 °C), the materials were water quenched at 100 °C or 20 °C to produce slow quench (~2 °C/s) and fast quench (~100 °C/s) microstructures, respectively. In order to achieve equivalent yield strength levels for the two quench conditions in T76 overaged tempers of commercial relevance (Section III–B), the fast quench material had to be aged slightly longer, with the following treatments then being utilized: 10 hours at 118 °C + 20 hours at 170 °C for the slow quench materials, and 10 hours at 118 °C + 28 hours at 170 °C for the fast quench materials.

Optical microscopy and image analysis were used to characterize grain structures and intermetallic contents. In order to characterize the distribution of coarse grain boundary precipitates, samples of each microstructural state were examined using the backscattered electron mode of a JEOL* JSM 6400 scanning electron microscope (SEM), successfully resolving boundary particles down to ~0.1 μm. Samples were polished to a 1/4 μm finish using diamond paste rather than colloidal silica to avoid the etching of the precipitates. Transmission electron microscope (TEM) foils were prepared using standard procedures: ~300-μm-thick samples of each microstructure were cut from the (LS) plane, ground to ~150 μm, and electropolished in a Struers Tenupol II using 30 pct nitric acid in methanol at −30 °C, at a voltage of 12 V. In addition to standard SEM and optical fractography, simultaneous observations of fracture surface features and corresponding underlying microstructures were made in the SEM at specimen midthicknesses where fracture surfaces had been protected with a lacquer coating prior to sectioning, polishing, and etching, with the coating then being removed prior to edge-on SEM observation. Sections of arrested crack specimens were also examined.

*JEOL is a trademark of Japan Electron Optics Ltd., Tokyo.

B. *Mechanical Testing*

Longitudinal tensile properties were evaluated using standard monotonic tensile tests according to ASTM E646. Toughness tests were carried out in longitudinal-transverse (L-T) and short-longitudinal (S-L) orientations in accordance with ASTM E399, although a nonstandard compact shear specimen (CSS) geometry was used,[15] as mixed-mode failure behavior was also of interest in these materials. The present article considers only mode I results however, where the CSS specimen is loaded in a simple uniaxial manner, analogous to a single edge notched tension specimen. Given materials limitations on the specimen size (corresponding to a width (W) of 40 mm and thickness (B) of 20 mm for both material orientations), the results were not all strictly valid as K_{IC} and are therefore given here as K_Q values (B and W values fell to ~1.5 $(K_Q/\sigma_y)^2$ in one case, while the remainder corresponded to B, $W \geq 2\ (K_Q/\sigma_y)^2$). The fact that all specimens were of the same geometry and yield strength level justifies their comparison.

Table I. AA7010 Plate Compositions (Weight Percent)

Material	Zn	Cu	Mg	Zr	Mn	Si	Fe	Cr
Unrecrystallized	6.03	1.55	2.37	0.11	0.01	0.04	0.06	0.01
Partially recrystallized	6.16	1.59	2.34	0.11	0.015	0.06	0.1	0.01

III. RESULTS

A. *Microstructural Characterization*

Key microstructural features for the various materials are summarized in Table II, with typical micrographs of the unrecrystallized and partially recrystallized microstructures being shown in Figure 1. From Table II, it may be seen that a recrystallized fraction range of 0 to ~20 pct was achieved, representative of values obtained during standard industrial processing. It is significant to note that intermetallics were predominantly located at grain boundaries in the unrecrystallized material and within recrystallized grains in the recrystallized material.

As may have been expected, significant coarse grain boundary precipitation occurred in both slow quench materials (Figure 2). Subgrain boundary precipitation was also noticeable in the slow quench specimens using the SEM, but was not resolvable in the fast quench specimens. For a given quench condition, similar grain boundary decoration was observed in the recrystallized and unrecrystallized conditions. Furthermore, the nature of the grain boundary (*viz.* lying between recrystallized and unrecrystallized grains, two recrystallized or two unrecrystallized grains) had no obvious systematic effect on grain boundary precipitation.

Subgrain boundary precipitation in both slow quench microstructures (partially recrystallized and unrecrystallized) was bimodal (Figure 3(a)): the dominant population was relatively coarse, with an average precipitate length of ~250 nm; a secondary population of finer precipitates (average length was ~30 nm) was also seen. Area coverage of the boundaries was relatively high (>0.5). The TEM characterization of precipitation in 7xxx Alloys by previous authors[16] indicates that these precipitates are variants of the η phase. Sub-boundaries were surrounded by a PFZ, with an average half-width of ~30 nm (variations of the order of ±10 nm).

In the fast quench microstructures, there was a dense population of sub-boundary precipitates, which were similar to the finer sub-boundary precipitates observed in the slow quench condition (average length ~30 nm), but more numerous (Figure 3(b)). Boundary coverage was again high. Sub-boundaries were generally surrounded by PFZs, whose average half-width was similar to that in the slow quench materials, *i.e.*, ~30 nm.

Bulk η' strengthening precipitation, as seen in Figure 3, was similar for the different microstructures (fast quench and slow quench), confirming, *a posteriori*, that the differences in the aging treatments had not produced significant variations in matrix strengthening. Coarse η precipitation was observed in the matrix of the slow quench materials (Figure 4) in both recrystallized and unrecrystallized areas, presumably forming heterogeneously on β' (Al_3Zr) dispersoids during the quench.[17,25] The shape and size of these precipitates were similar to those observed on the subgrain boundaries of the slow quench materials (~200 nm on average).

B. *Mechanical Properties*

Longitudinal tensile test data are presented in Table III. The results show that yield strengths were reasonably constant for all four materials (all within ~6 pct of each other).

Table II. Microstructural Characterization of the Different Materials

Microstructural Features	Fast Quench (100 °C/s)	Slow Quench (2 °C/s)
Grain structure	unrecrystallized microstructure: recrystallized fraction = 0 pct primary grain size (μm): S = 33 subgrain size (μm): S = 7, L = 10, T = 10 area fraction of intermetallics = 0.7 pct partially recrystallized microstructure: recrystallized fraction = 18 pct primary grain size (μm): S = 36 recrystallized grain size (μm): S = 35, L = 84, T = 80 subgrain size (μm): S = 2, L = 4, T = 4 area fraction of intermetallics = 0.9 pct	
Grain boundary structure	fine precipitation length ~0.3 μm a few coarse precipitates >1 μm	coarse precipitation length ~1 μm density ~0.3 μm^{-1}
Subgrain boundary structure	population of small precipitates length ~30 nm PFZ width ~60 nm	two populations of precipitates: large: length ~250 nm small: length ~30 nm PFZ width ~60 nm
Matrix precipitation	copious η'/η precipitation	copious η'/η precipitation course heterogeneous η precipitates (length ~200 nm)

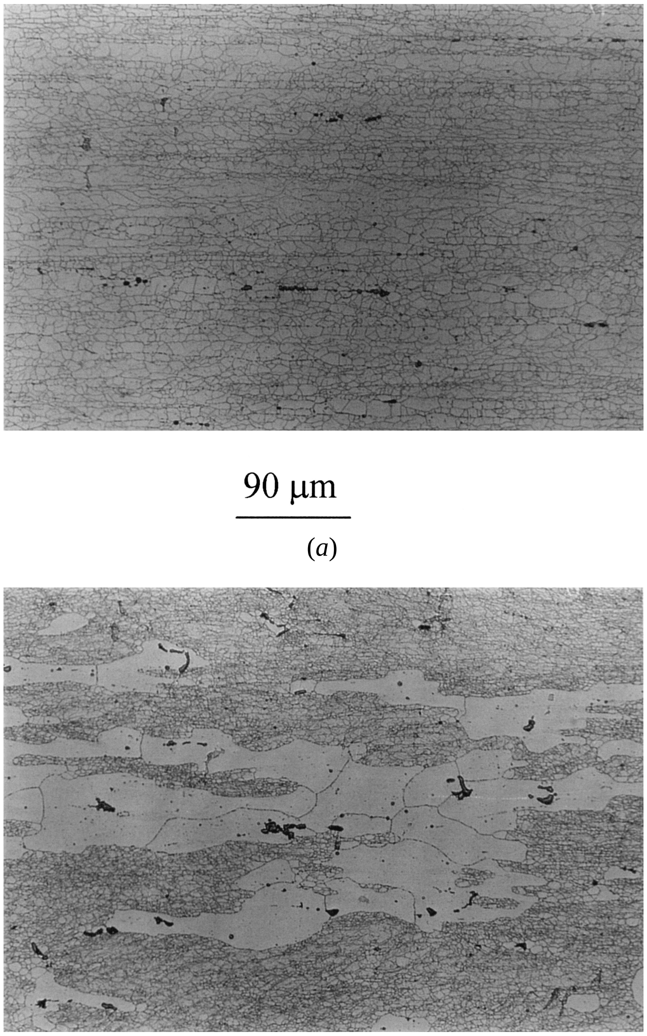

Fig. 1—Microstructure of the (*a*) unrecrystallized and (*b*) recrystallized materials (sections in the L-S plane; orthophosphoric acid etch).

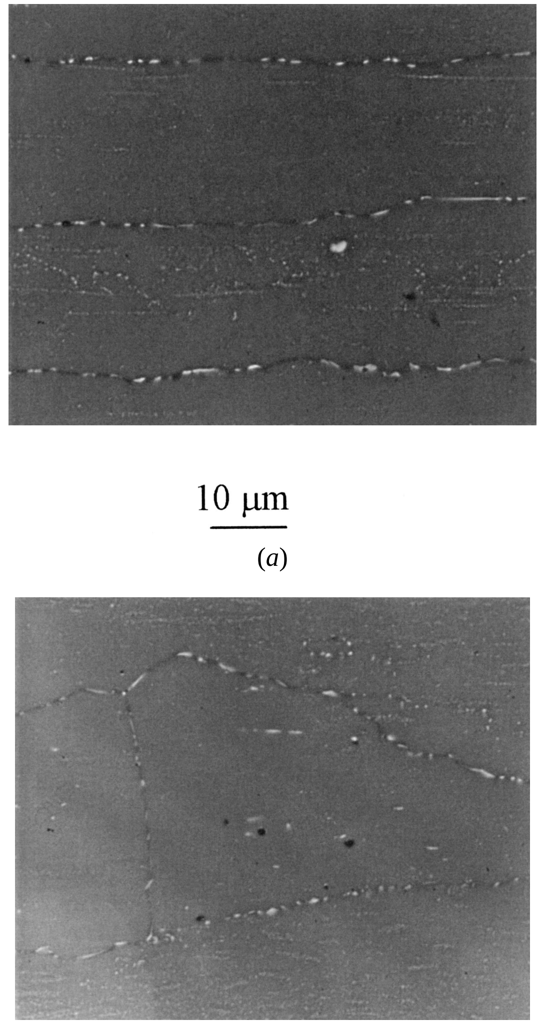

Fig. 2—Grain boundary precipitation in (*a*) USQ and (*b*) PRSQ microstructures (imaged in SEM backscattered electron mode after 1/4 μm diamond polish).

Fracture Toughness

a. *L-T orientation*

L-T fracture toughness data are illustrated in Figure 5. Decreasing quench rate produced a significant reduction of toughness (around 20 pct) in both grain structures, with the partial recrystallization giving a consistent decrease in toughness of ~11 pct for both quench conditions. Within the expected scatter in toughness measurements, no significant difference in quench sensitivity was identifiable between the unrecrystallized and partially recrystallized materials.

b. *S-L orientation*

S-L fracture toughness data are illustrated in Figure 6. The effect of quench rate was significant in both recrystallized and unrecrystallized microstructures, with the unrecrystallized material being significantly more quench sensitive, exhibiting a 33 pct drop in toughness compared to 23 pct for the partially recrystallized material. While a 15 pct drop in toughness due to recrystallization was evident for the fast quench condition (*i.e.*, similar to the L-T orientation tests), no equivalent effect was seen in the slow quench materials.

The presence of intermetallics is known to have a detrimental effect on the fracture properties of high strength aluminum alloys. While efforts were made to ensure as close comparability within the test matrix as possible, Table II shows some variation in intermetallic content between the materials. Based on Eq. [1], such a difference in intermetallic content is estimated to have an effect on K_{IC} of ~4 pct, *i.e.*, a relatively minor effect given a typical scatter in K_Q values of 3 pct. The observed trends within the data are therefore considered to be essentially valid.

C. *Fractography*

1. *L-T orientation*

Fracture surfaces varied significantly between the different material conditions, with the major effects being outlined in Table IV. Typical micrographs are presented in Figures 7 through 9 and may be summarized as follows.

a. *Unrecrystallized fast quench material*

Fracture surfaces were relatively ductile and were characterized by large dimples of the order of 10 to 50 μm in

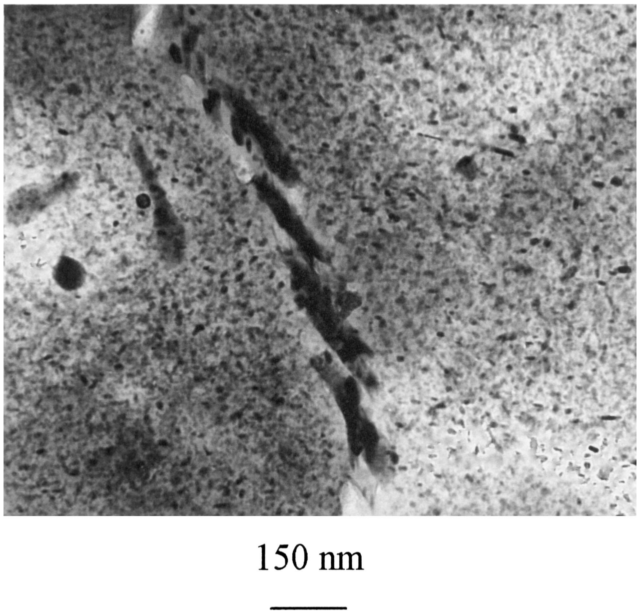

(*a*)

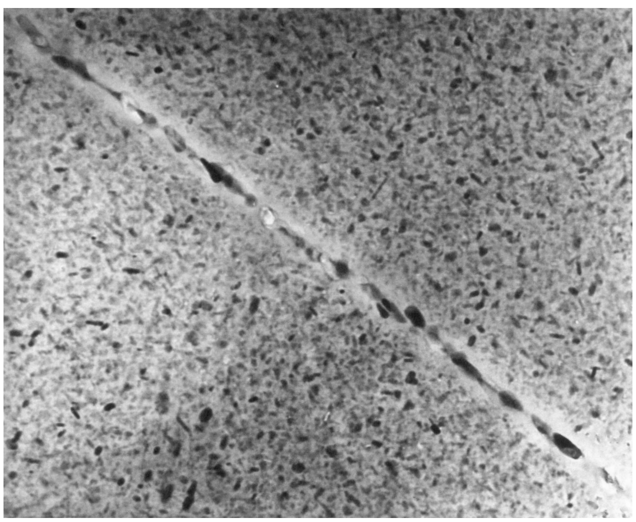

(*b*)

Fig. 3—Subgrain boundary precipitation in the (*a*) slow quench and (*b*) fast quench microstructures.

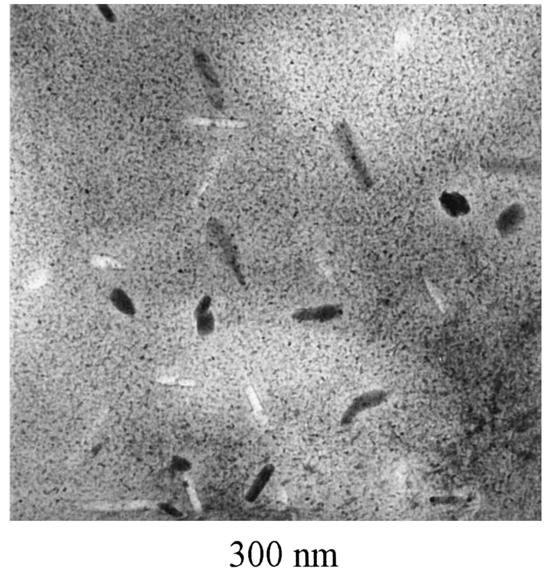

Fig. 4—Heterogeneous matrix precipitation in the slow quench microstructures.

Table III. Tensile Properties of the Four Different Microstructures

Microstructure	0.2 Pct Yield Stress (MPa)	Ultimate Tensile Strength (MPa)	Elongation at Fracture (Pct)
PRFQ	428	495	12.0
PRSQ	438	505	11.3
UFQ	430	490	13.4
USQ	458	520	12.8

diameter (Figure 7(a)). Aggregates of intermetallics could often be seen within these dimples. The failure mode was predominantly transgranular, although occasional intergranular failure along grain boundaries in the LT plane was noted.

b. *Unrecrystallized slow quench material*

Fracture surfaces exhibited a very different character compared to the same material in the fast quench condition (Figures 7(a)(b)). While crack growth was again mainly transgranular, extensive void growth was not observed at intermetallic particles. Failure predominantly occurred *via* planes running parallel to, but twisted about, the crack growth direction. Such through-thickness shear planes were covered with fine dimples, about 1 μm across (Figure 8). Some intergranular failure was observed linking shear planes from adjacent grains, although there was no delamination of the boundaries into the specimen bulk.

c. *Partially recrystallized fast quench material*

In keeping with the unrecrystallized material in the fast quench condition, fracture surfaces in this case were very ductile, exhibiting dimples (10 to 50 μm in diameter) around aggregates of intermetallics (Figure 7(c)). Fracture was primarily transgranular both in recrystallized and unrecrystallized grains. In keeping with the initiation of voids at intermetallic particles (which was clearly seen ahead of the crack in arrested crack sections), preferential propagation *via* recrystallized grains was evident. This was confirmed by quantitative optical measurements of the proportion of crack growth, which was through recrystallized areas, this figure being larger than the background recrystallized grain content (Table V).

d. *Partially recrystallized slow quench material*

Fracture surface appearance was intermediate between that of the USQ and PRFQ conditions (Figure 7): unrecrystallized regions mainly failed transgranularly *via* shear planes covered with fine dimples ($\sim$1 μm) as in USQ material, whereas the recrystallized grains predominantly failed transgranularly by ductile void growth on intermetallics, as in the PRFQ material (Figure 9(b)). Intergranular failure along recrystallized grains was also evident. The role of the intermetallics as void initiation sites was again confirmed from the arrested crack tests, with preferential propagation occurring through recrystallized grains (Figure 9 and Table V).

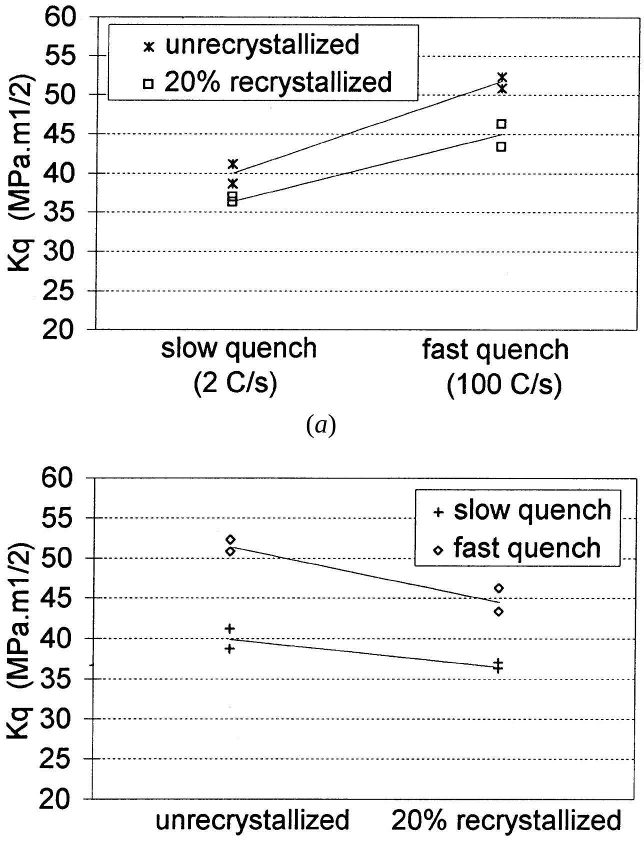

Fig. 5—Fracture toughness results for the L-T orientation showing the effect of (*a*) quench rate and (*b*) recrystallized fraction.

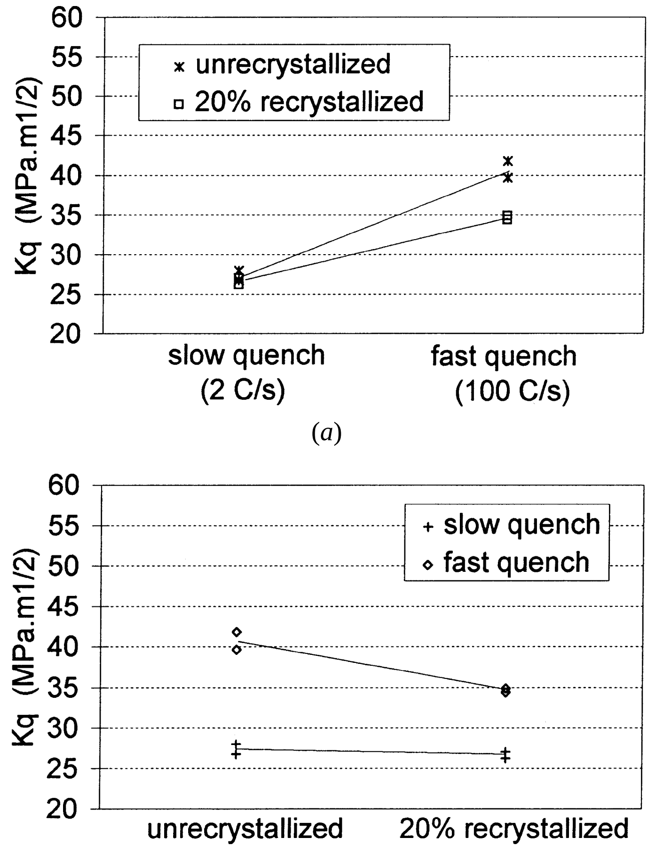

Fig. 6—Fracture toughness results for the S-L orientation showing the effect of (*a*) quench rate and (*b*) recrystallized fraction.

2. *S-L orientation*

Overall failure characteristics for the S-L orientation tests are outlined in Table IV. Intermetallics were particularly evident on the fracture surfaces of the S-L specimens (higher area coverage than the L-T tests), presumably due to the clustering of the intermetallics in the rolling plane of the materials. Typical micrographs for the different microstructures are presented in Figures 10 through 13 and may be summarized as follows.

a. *Unrecrystallized fast quench material*

Fracture surfaces exhibited a mixture of features (Figure 10(a)): ductile areas with numerous large ($\geq$10 μm in diameter) but relatively shallow dimples associated with intermetallics, and flat intergranular areas characterized by a fine (less than 1 μm) population of shallow dimples. Intergranular areas were located at different levels, linked by transgranular steps.

b. *Unrecrystallized slow quench material*

Large intergranular areas covered most of the fracture surface (Figures 10(b)). Numerous aggregates of intermetallics were also identifiable, although little associated void growth was evident, contrary to the UFQ condition. The intergranular areas were again linked by transgranular steps, but less frequently than in the UFQ tests. Crack path sections showed that ridges commonly linked adjacent grain boundaries, *i.e.*, crossing only one grain in the S direction (Figure 11). Higher magnification examination of the intergranular areas showed they were covered with shallow dimples, of ~1 to 5 μm in diameter, *i.e.*, larger than in the UFQ condition (Figure 12). Coarse grain boundary precipitates (~0.5 to 1.5 μm) could be seen within some of these dimples.

c. *Partially recrystallized fast quench material*

This microstructure exhibited the most obviously ductile fracture surface of the S-L tests. Large dimples (>10 μm), commonly associated with intermetallics, covered much of

Table IV. Summary of the Failure Mechanisms Identified in the Different Specimen Orientations and Microstructural Conditions, with a Semiquantitative Indication of the Proportion of Each Mechanism (indicated by •)

Specimen Orientation	Microstructural Condition	Failure Mechanisms
L-T	UFQ	primary voiding ••••
	USQ	transgranular shear ••••
	PRFQ	primary voiding ••••
	PRSQ	primary voiding • / transgranular shear •••
S-L	UFQ	primary voiding •• / grain boundary ductile failure ••
	USQ	grain boundary ductile failure ••••
	PRFQ	primary voiding ••• / grain boundary ductile failure •
	PRSQ	primary voiding • / grain boundary ductile failure •••

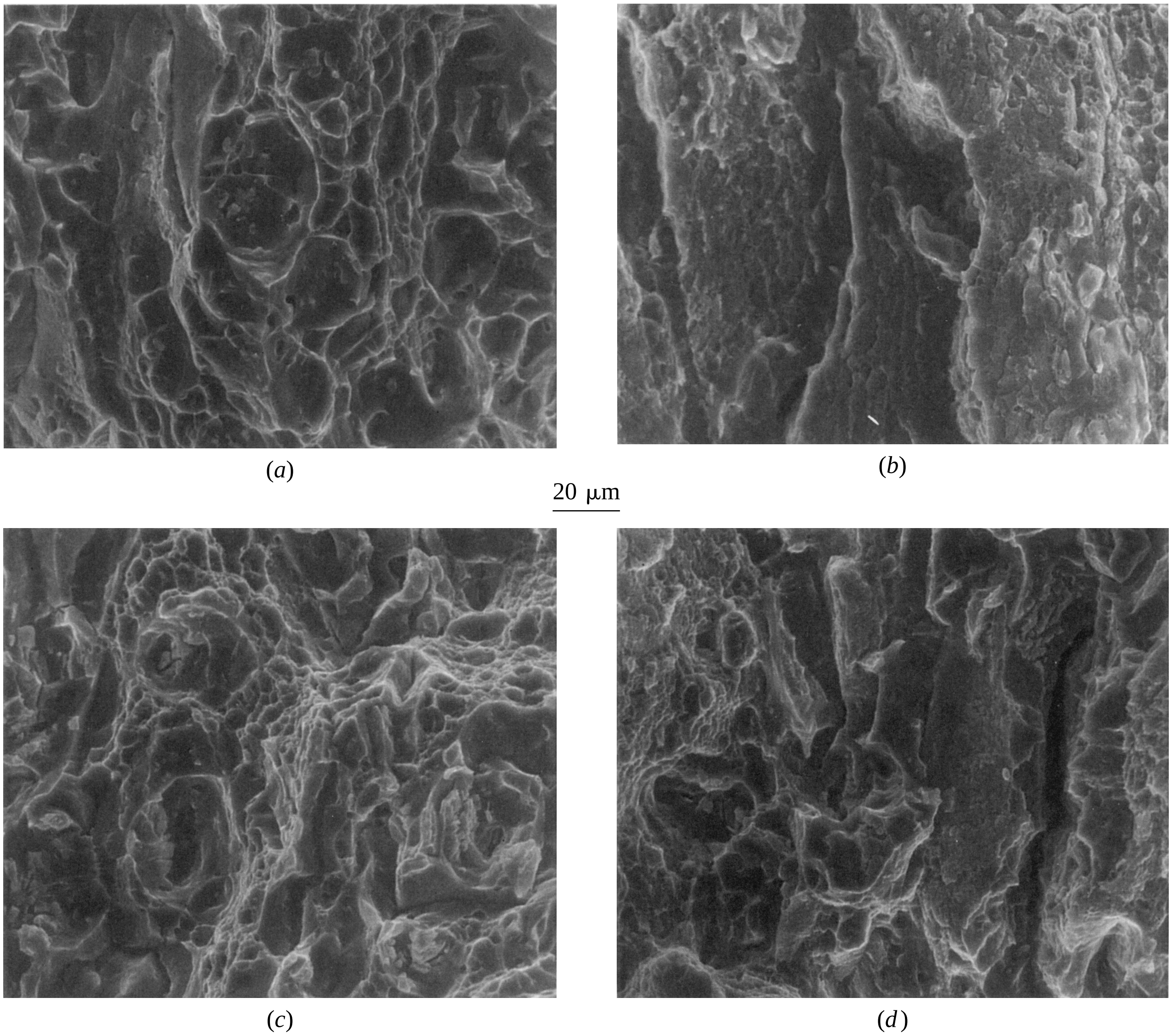

Fig. 7—Fracture surfaces of the different microstructures tested in the L-T orientation: (*a*) unrecrystallized / fast quench, (*b*) unrecrystallized.slow quench, (*c*) 20 pct recrystallized / fast quench, and (*d*) 20 pct recrystallized / slow quench. Extensive void growth has occurred in the fast quench conditions on the intermetallics. In the slow quench conditions, transgranular shear planes are the dominant feature.

the surfaces (Figure 10(c)). Observation of the arrested crack specimens showed that failure on intermetallics was related to transgranular propagation of the crack through the recrystallized grains (Figure 13(a)). This mechanism was extensive (50 pct of crack length, Table V), but intergranular failure along recrystallized grains was also significant (30 pct of crack length). Even in the latter case, however, extensive void growth generally occurred at the intermetallics within the body of individual recrystallized grains, in addition to boundary failure.

d. *Partially recrystallized slow quench material*

Fracture surfaces were characterized by two types of feature (Figure 10(d)): intergranular areas, similar to those observed in the USQ condition; and ductile areas, exhibiting large dimples ($\sim$10 μm) associated with aggregates of intermetallics. Crack path examination confirmed (Figure 13(b)) that the latter was related to transgranular fracture through the recrystallized grains (25 pct of crack length, Table V), consistent with the location of intermetallics within the recrystallized grains. Intergranular failure *via* recrystallized grains, however, was the predominant failure mode (55 pct of crack length).

IV. DISCUSSION

A. *Failure Micromechanisms*

1. *L-T Orientation Tests*

Two failure mechanisms predominate in the L-T orientation tests: coarse primary voiding and transgranular shear. The former represents a classical relatively high energy ductile failure mode, with extensive deformation associated with void growth from the large intermetallic particles, consistent with the higher fracture resistance of the fast quench materials (recrystallized and unrecrystallized, Table IV and Figure 14). As noted in Section I, the shear band failure that was evident in the lower toughness slow quench materials may

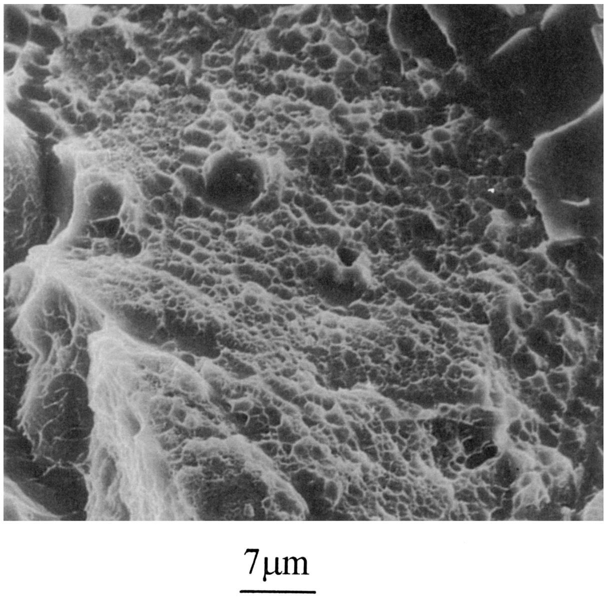

Fig. 8—High-magnification micrograph of transgranular shear plane showing characteristic distribution of fine dimples (slow quench microstructure).

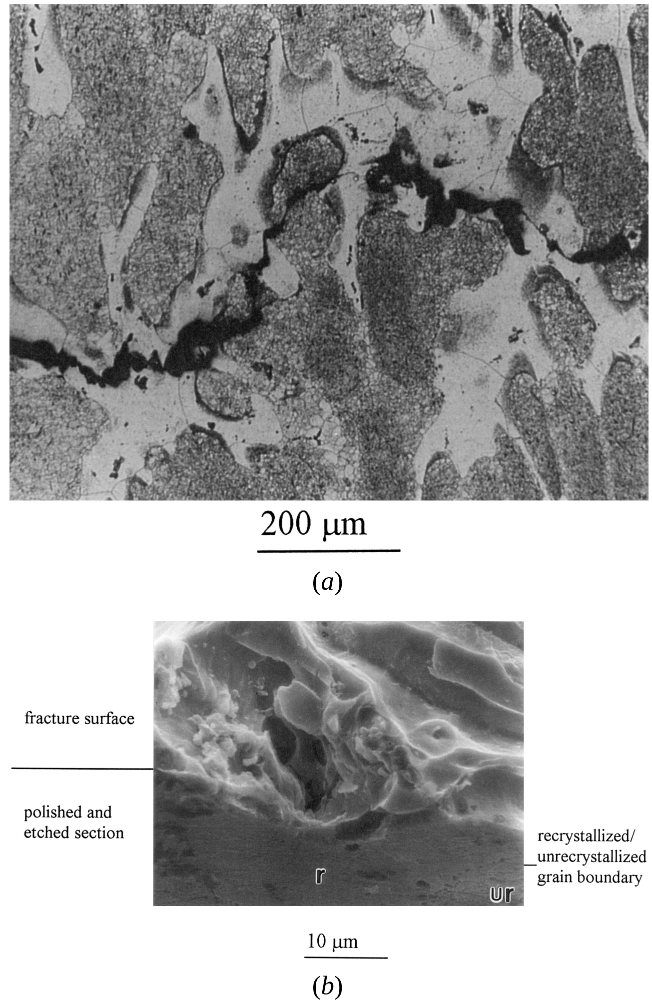

Fig. 9—(*a*) Optical section (L-T plane) of a PRSQ specimen tested in the L-T orientation illustrating preferential crack propagation within the recrystallized areas. (*b*) Edge-on SEM micrograph of the fracture surface and a polished and etched section showing a large dimple formed on intermetallics within a recrystallized grain. "r" and "ur" indicate recrystallized and unrecrystallized areas, respectively.

be associated with void sheet formation at dispersoid particles. In this work, it is evident that the Zr containing β' dispersoids present in AA7010-T76 did not in itself induce shear band failure since it did not occur in the fast quench materials. This is consistent with Chen and Knott[7] identifying a reduced intrinsic susceptibility of β' dispersoids to shear fracture with their relatively small size as dispersoids, spherical morphology/low aspect ratio, and matrix coherence (for unrecrystallized grains at least). While the exact processes associated with the formation and separation of shear bands are open to discussion[7,18,19] (particularly regarding the contributions of matrix flow character, local mechanical instabilities, and void initiation/growth to the shear localization process), it is clear that the intrinsic matrix flow character of the present materials was essentially constant, and increased susceptibility to shear failure in the slow quench materials must then be attributed to the intragranular precipitation that occurred in the slow quench materials, with the observed size and morphologies of these precipitates approaching that of the Cr containing dispersoids seen to crack during plastic deformation in other 7xxx-series alloys.[7,20,21] Given the similarity of the coarse intragranular precipitates and the intersubgranular precipitates observed in the slow quench materials, some contribution of subgrain particles to shear band failure would also appear possible. Surface corrugations of the order of the subgrain size were indeed evident on some shear fracture regions (*i.e.*, potentially indicative of intersubgranular failure), although the scale and morphology of the subgrains and local deformations during fracture make it difficult to quantify the effect. Many shear failure regions were also seen to be very planar, consistent with a truly transgranular failure mode. In these cases, it is interesting to note possible contributions to failure of sub-boundary particles that are intersected by a transgranular shear plane. Given the observed linear intercept separations for the intragranular coarse precipitates were of the order of 1 to 2 μm, it may be seen that a sub-boundary diameter of the order of a few microns may provide an appreciable contribution to the number of void initiating particles sampled along a given shear plane (independent of failure specifically following the subgrain boundaries). Potential implications of such behavior are considered later.

2. *S-L Orientation Tests*

In terms of the S-L orientation tests, coarse primary voiding and grain boundary ductile failure were the two main failure mechanisms. In keeping with the L-T tests, the former was most significant in the fast quench conditions (Table IV and Figure 15). A decrease in quench rate again favored a more localized failure mode (*i.e.*, grain boundary ductile failure), with exposure of grain boundaries to the maximum crack tip opening stresses in the S-L orientation clearly favoring boundary failure over the shear band separation that occurred in the L-T slow quench tests. The present TEM examination of the fast and slow quench microstructures showed similar PFZ widths and matrix strengthening precipitates, discounting any associated influences on boundary failure behavior. Boundary precipitation therefore must have exerted the primary influence on boundary failure (*i.e.*, as opposed to PFZ width or matrix/PFZ strength differential),

Table V. Measurements of the Linear Fraction of the Crack Propagating through Recrystallized Areas for Different Specimen Orientations and Microstructures

Orientation	Microstructure	Linear Recrystallized Fraction of the Crack (L_{rex})
L-T	PRFQ	>40 pct (includes intergranular and transgranular)
L-T	PRSQ	>54 pct (includes intergranular and transgranular)
S-L	PRFQ	50 pct transgranular, 30 pct intergranular
S-L	PRSQ	25 pct transgranular, 55 pct intergranular

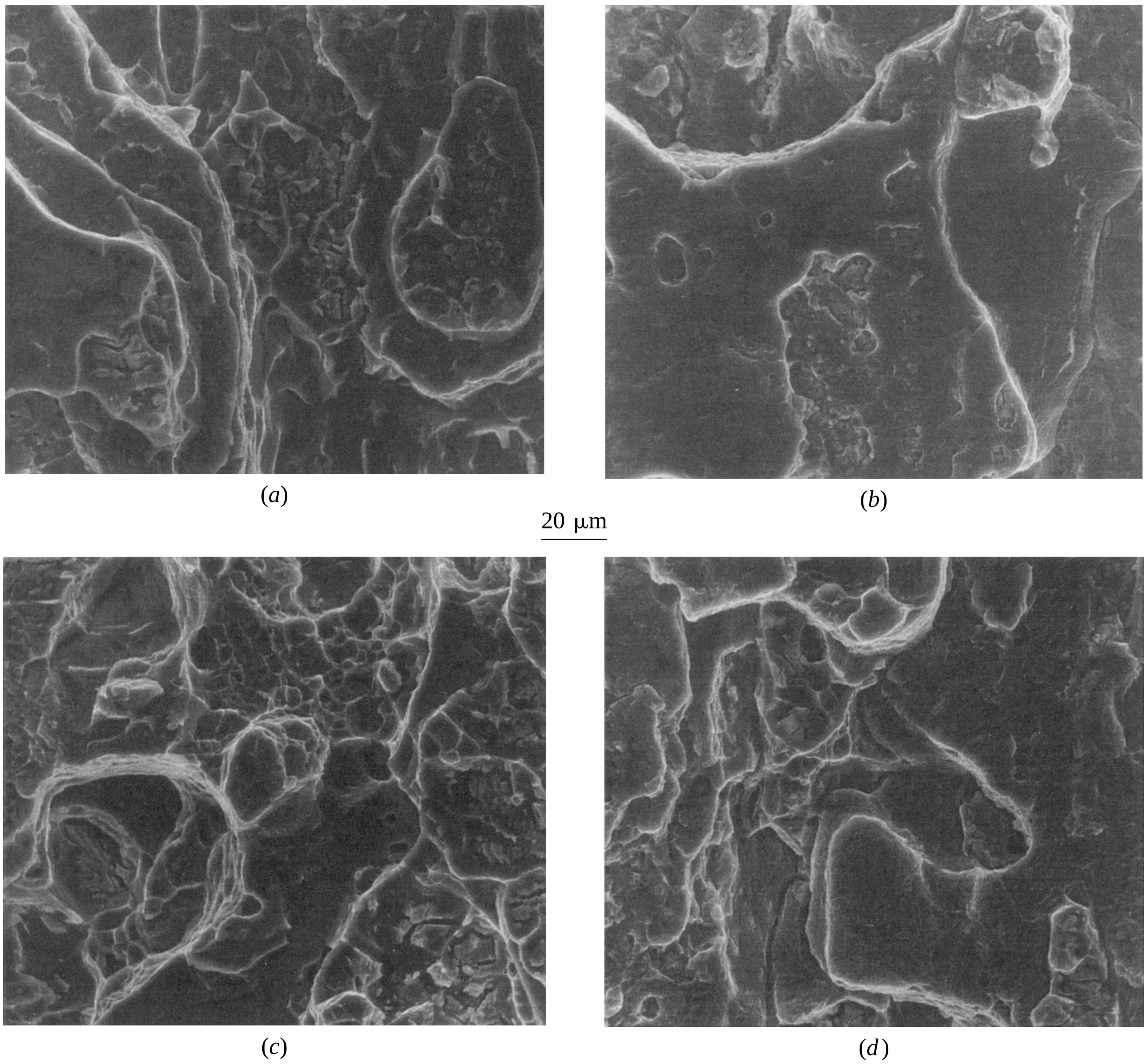

Fig. 10—Fracture surfaces of the different microstructures tested in the S-L orientation: (*a*) UFQ, (*b*) USQ, (*c*) PRFQ, and (*d*) PRSQ. Grain boundary failure and primary void growth at intermetallics are evident in the fast quench conditions, with more extensive intergranular failure occurring in the slow quench materials.

with the incidence of coarse boundary precipitation in slower quench materials being reflected in coarser boundary voids. In the absence of boundary area coverage measurements, it is not possible to further quantify boundary precipitate effects on intergranular failure and toughness levels, although it is clear that increased particle size may contribute to failure in keeping with the results of Kirman.[27]

3. *Recrystallization Effects*

Observations of the L-T and S-L specimens, based on SEM examination of the fracture surfaces and optical sections of arrested crack specimens, showed that recrystallized grains were a favored crack path. Thompson and Zinkham[14] reports values of the plane stress fracture toughness of various 7075 type alloys with different grain structures and

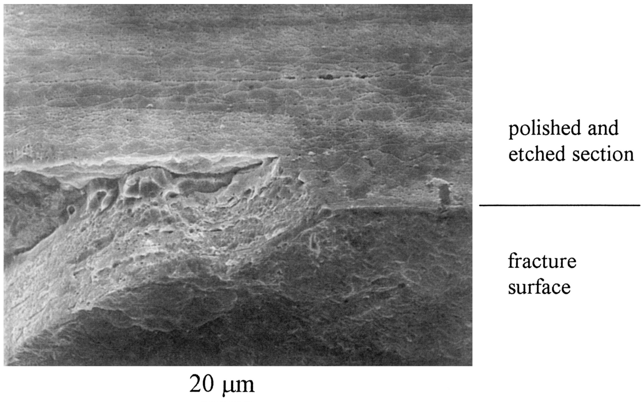

Fig. 11—Edge-on SEM micrograph (fracture surface and polished section) of the unrecrystallized/slow quench specimen tested in the S-L orientation, showing two intergranular areas linked by a transgranular step.

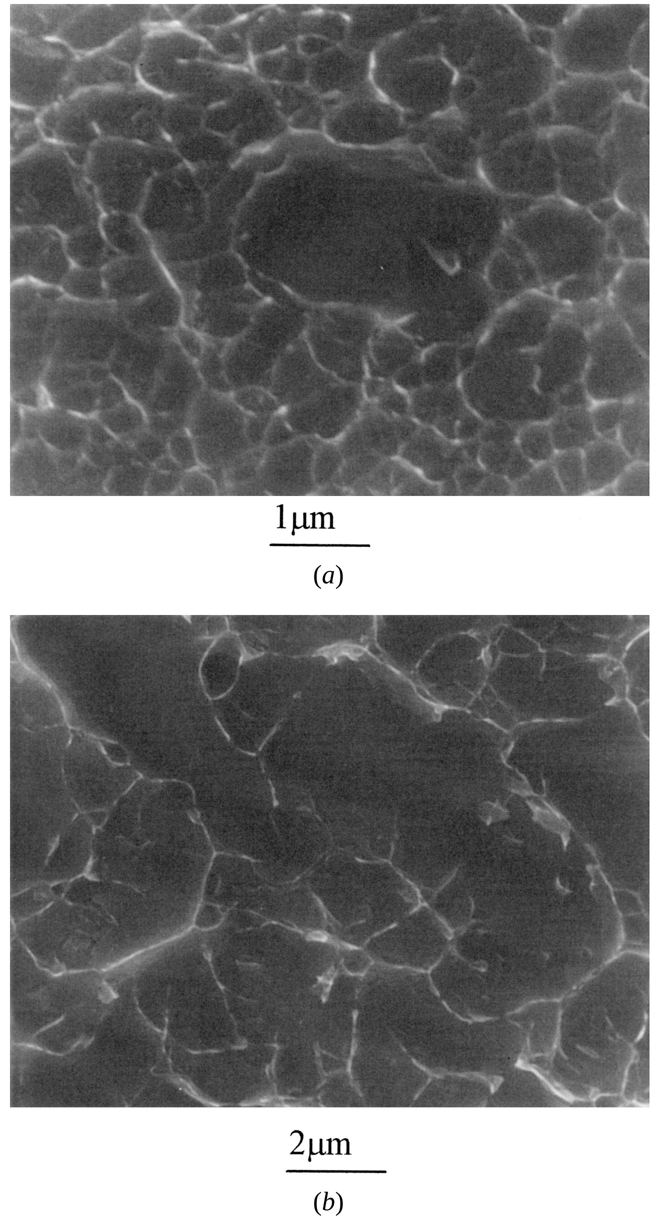

Fig. 12—High-magnification micrographs of the intergranular areas on the fracture surfaces of specimens tested in the S-L orientation: (*a*) fast quench and (*b*) slow quench microstructure. Larger dimples are evident in the slow quench microstructure.

relates the detrimental effect of recrystallization to the occurrence of intergranular crack propagation. Similarly, Staley[22] suggests that recrystallized grains are preferential crack paths because they introduce high-angle boundaries that promote coarse heterogeneous precipitation, especially during slow quench conditions. In the present tests, failure at recrystallized grains was predominantly transgranular in the L-T orientation in both fast quench and slow quench conditions. In the S-L orientation/fast quench material tests, the proportion of intergranular failure at the recrystallized grains became more significant (compared to the L-T tests), although the effect of partial recrystallization was to actually increase the proportion of transgranular failure over that in the unrecrystallized samples. Intergranular failure became predominant in the slow quench/S-L condition, although the proportion of transgranular failure remained significant in the partially recrystallized alloy. Overall, it may be seen that while recrystallization was consistently detrimental to toughness, intergranular embrittlement did not consistently explain this behavior. The present work further showed that, for a given quench condition, similar precipitation occurred on the different types of grain boundaries (*i.e.*, recrystallized/recrystallized, recrystallized/unrecrystallized, *etc.*). In a given quench condition, the intrinsic propensity for intergranular failure would then appear to be similar for recrystallized and unrecrystallized grains. It may also be noted that the recrystallized grains were no larger than the primary grains and therefore should not be "weakened" by the grain size dependency of differential grain boundary straining implied in Eq. [4].

In terms of crack path preferentiality between recrystallized and unrecrystallized grains (independent of being inter- or transgranular), it is valuable to consider the role of intermetallics as primary void formation sites. This was observed directly on the sections of arrested crack specimens, with failure ahead of the main crack front initially occurring at the intermetallics within the recrystallized grains in the partially recrystallized material. As such, any subsequent crack growth will preferentially involve the recrystallized grains, independent of whether the recrystallized grains are actually intrinsically stronger or weaker than the surrounding unrecrystallized material. With recrystallized grains commonly acting as transgranular primary voiding sites, as opposed to intergranular failure sites, a question then arises in how to explain the detrimental effect of recrystallization on fracture. Crack propagation modes and toughness levels in the present materials are dependent on the extent to which primary void growth continues prior to a secondary failure mode (*i.e.*, intergranular or shear band failure), causing coalescence. Since primary voiding at intermetallics was a dominant failure mechanism in the fast quench conditions and there was no indication of preferential intergranular failure between the recrystallized and unrecrystallized materials, a detrimental effect of recrystallization on toughness suggests that primary void initiation and growth may be specifically "assisted" within the recrystallized grains, rather than involving grain boundary failure mechanisms. Such an effect does not appear to have been discussed within the literature. Of the potential metallurgical rationalizations, it is interesting to note that the partially recrystallized material

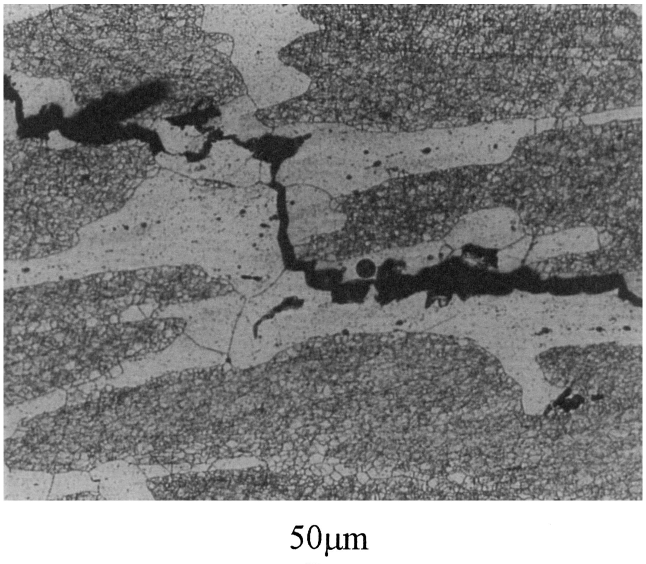

(*a*)

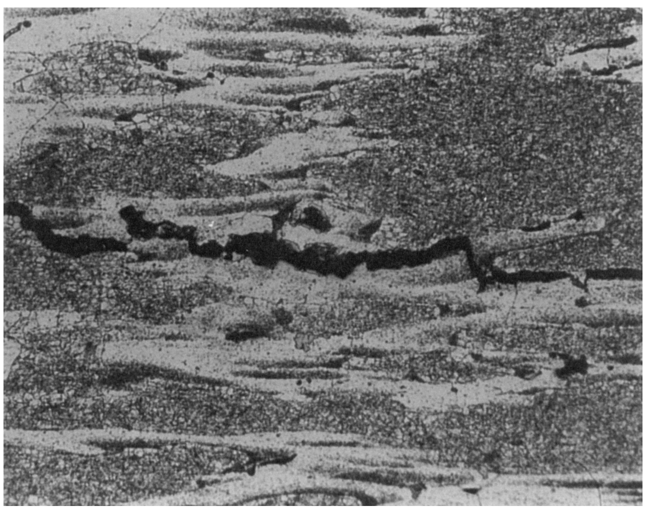

(*b*)

Fig. 13—Optical sections (S-L plane) of partially recrystallized specimens tested in the S-L orientation: (*a*) fast quench and (*b*) slow quench.

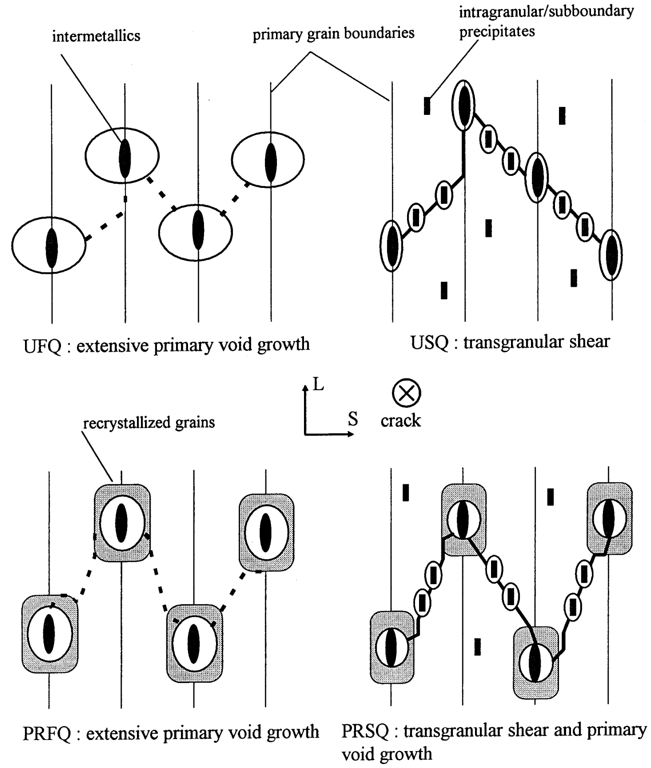

Fig. 14—Schematic diagrams showing the dominant failure mechanisms in the different microstructures for the L-T testing orientation (crack propagation direction perpendicular to the page).

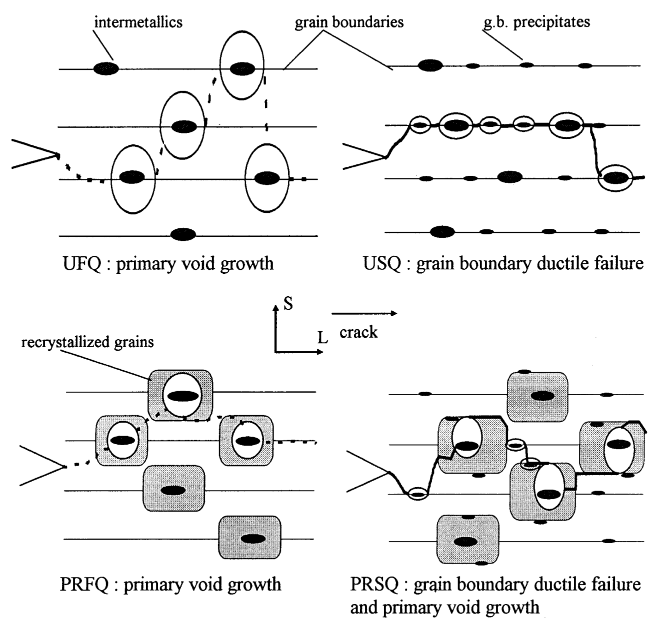

Fig. 15—Schematic diagrams showing the dominant failure mechanisms in the different microstructures for the S-L testing orientation. Crack propagation is in the plane of the page.

represents a composite system of recrystallized grains within an unrecrystallized "matrix" (as opposed to the more fully recrystallized materials often discussed in previous recrystallization investigations). As such, void initiation and/or growth may be promoted by differential straining of recrystallized grains due to the local absence of substructure and any associated variations in flow stress and/or work hardening characteristics. Such behavior represents a reasonably complex elastic/plastic deformation problem. In the first instance, it may be noted that given a reasonable Petch–Hall constant for an aluminum substructure (~0.05 MPa$\sqrt{\text{m}}$[23]), the absence of a ~3-μm substructure (characteristic of the change between recrystallized and unrecrystallized regions in the partially recrystallized material) corresponds to a ~30 MPa reduction in local flow stress. Such a softening may be expected to localize strain within the recrystallized grains, accelerating void growth. While the presence of sub-boundary PFZs might also be expected to have some softening effect within the unrecrystallized regions, it is clear that the local presence or absence of substructure may have an important influence on flow behavior in the failure critical environment of the large intermetallic particles.

Of the individual and combined effects of quench rate and recrystallization on toughness in the present data, the quench sensitivity of the unrecrystallized material in the S-L orientation is distinctive (-33 pct in K_Q compared to -23 pct for the partially recrystallized material). Dorward and Beerntsen[12] report a similar trend in a 7050 material in the L-T orientation (note that our results in the L-T orientation do not show this effect). They proposed that this effect was due to precipitation on the subgrain boundaries in the unrecrystallized material, which exhibited a more strongly developed subgrain structure. However, TEM observation of sub-boundary precipitation in the USQ and the PRSQ microstructures in the present materials showed no such effect. A more probable explanation of the S-L quench sensitivity of the unrecrystallized materials in this work may be based on the synergistic effect of intermetallics and coarse grain boundary precipitates both favoring intergranular failure in the slow quenched unrecrystallized microstructure.[19] With secondary void formation acting as the effective limiting factor in primary void growth, it may be seen that intermetallics being located along planes of secondary void initiation sites (*i.e.*, the grain boundaries in the unrecrystallized material) may accelerate the onset of secondary void linkage. This is then consistent with reduced quench sensitivity in the partially recrystallized S-L orientation tests, where primary void formation occurs off the grain boundaries (*i.e.*, within the recrystallized grains), and behavior in the L-T orientation tests, where the secondary void formation process (shear band failure) is not specifically related to grain boundary location.

B. *Implications of Multiple Failure Mechanisms*

A number of the tests reported here exhibited distinct combinations of failure modes. An approach taken by Sugamata *et al.*[24] to modeling mixed failure mechanisms in Al-Li alloys suggests that overall fracture toughness levels may be expressed as a simple area weighted linear summation of toughnesses associated with individual failure modes. In their work, grain boundary and shear band failure were specifically considered, both being highly localized failure processes where interactions between mechanisms may indeed be relatively limited. As such, synergistic effects may not be accounted for, such as the interaction between grain boundary intermetallics and boundary precipitates thought to occur in S-L tests of the slow quenched unrecrystallized material. In terms of the L-T orientation, a lower quench rate and partial recrystallization resulted in the incidence of transgranular shear within the unrecrystallized grains, and primary voiding within the recrystallized grains, resulting in the lowest measured toughness for this orientation. A toughness summation approach would suggest that, since the two main mechanisms occurred essentially independently in the USQ condition (transgranular shear) and in the PRFQ condition (primary voiding), the resulting K_Q could be expressed as

$$K_Q^{\mathrm{PRSQ}} = X_{TS} K_Q^{\mathrm{USQ}} + X_{PV} K_Q^{\mathrm{PRSQ}} \qquad [5]$$

where X_{TS} and X_{PV} are the proportions of transgranular shear and primary voiding in the PRSQ condition ($X_{TS} + X_{PV} = 1$). The resulting intermediate fracture toughness value between those of the two single-mechanism conditions would necessarily then be an overprediction (Gokhale *et al.*[29] suggest that toughness contributions may also be summed as squared terms, which would indeed lead to a further overprediction). It is then interesting to consider that the intrinsic toughness associated with shear failure in the partially recrystallized microstructure may actually be lower than that measured in the unrecrystallized microstructure if the finer sub-boundary structure and associated precipitates contribute to shear band void formation. An estimate of the influence of particle density on void initiation within shear bands may be taken from Chen and Knott's work, as represented by Eq. [3]. For a 1.5 μm linear intercept separation of the large intragranular precipitates, the reduced mean interparticle separation due to the introduction of particle decorated subgrains of 9 and 3 μm diameter (*cf.* the unrecrystallized and partially recrystallized material) yields reductions in λ of 20 and 40 pct, respectively. Corresponding reductions in K_{IC} of $\sim$10 and 20 pct are then given by Eq. [3]. Chen and Knott's model for shear band failure is based on void initiation; however, coalescence controlled failure may also be assessed *via* the boundary shear failure analysis of Embury and Nes,[19] where the extent of stable growth that occurs for a planar array of voids is identified with the point where adjacent voids begin to overlap above and below the plane of shear. The local strain to plastic collapse, γ, is then estimated from $\gamma = \lambda/2h$, where λ is the interparticle separation, and h is the void initiating particle size. From this, crack tip strain controlled toughness models such as Eq. [2] also yield reductions in K_{IC} of $\sim$10 and 20 pct due to the introduction of 9 and 3-μm diameter particle decorated subgrains, respectively. From the analyses of Chen and Knott and Embury and Nes, K_Q^{USQ} in Eq. [5] may then be modified by a factor of $\sim$0.9 if the change in subgrain size does contribute additional particles to the shear band failure process in the unrecrystallized regions of the partially recrystallized material. While a number of simplifications and assumptions are involved in doing this, a predicted K_Q^{PRSQ} of 37.5 MPa$\sqrt{\mathrm{m}}$ is obtained (based on an estimated 3:1 ratio of shear to coarse void failure), corresponding closely to the measured value of 36.3 MPa$\sqrt{\mathrm{m}}$.

V. CONCLUSIONS

1. The effects of quench rate and recrystallization on the fracture toughness of AA7010-T76 plate have been studied in the L-T and S-L orientations for representative commercial microstructures identifying distinct micromechanical influences for each orientation.
2. Coarse heterogeneous η precipitation was identified on grain boundaries, subgrain boundaries, and within the matrix of slow quenched materials. The location of the large intermetallic particles was identified as critical during fracture, being mainly located within recrystallized grains in the partially recrystallized material and on grain boundaries in the unrecrystallized material.
3. A slow quench had a strong detrimental effect on fracture toughness in both L-T and S-L orientations. The drop in K_Q was consistent with a change in the dominant failure mechanism, from extensive primary void growth in the fast quench conditions to transgranular shear in the L-T slow quench conditions and grain boundary ductile failure in the S-L slow quench conditions. The changes in failure mechanism were correspondingly attributed to heterogeneous intragranular and intersubgranular precipitation in

the L-T orientation, and intergranular heterogeneous precipitation in the S-L orientation. A simple linear summation of fracture mechanism contributions to fracture resistance in the L-T orientation was shown to rationalize quench sensitivity in partially recrystallized material provided variations in subgrain size were taken into account.

4. Partial recrystallization had a detrimental effect on the fracture toughness in the L-T orientation for both quench conditions and in the S-L orientation for the fast quench condition. This effect could not be attributed to intergranular failure only. As such, a direct interaction is proposed between the local presence or absence of substructure around intermetallic clusters and their contribution to primary void growth.
5. In the S-L orientation, a high quench sensitivity was identified in the unrecrystallized microstructure. This was attributed to the synergistic location of intermetallics and coarse boundary precipitates in the unrecrystallized slow quench material, highlighting the role of micromechanical interactions that may occur between failure modes.

ACKNOWLEDGMENT

The authors wish to acknowledge the support of Pechiney CRV in carrying out this research.

REFERENCES

1. D.S. Thompson: *Metall. Trans. A*, 1975, vol. 6A, pp. 671-83.
2. G.T. Hahn and A.R. Rosenfield: *Metall. Trans. A*, 1975, vol. 6A, pp. 653-68.
3. J.R. Rice and M.A. Johnson: *Inelastic Behavior of Solids*, McGraw-Hill, New York, NY, 1970, pp. 641-72.
4. G.T. Hahn and A.R. Rosenfield: *ASTM STP 432*, 1968, pp. 5-32.
5. G.G. Garrett and J.F. Knott: *Metall. Trans. A*, 1978, vol. 9A, pp. 1187-1201.
6. D. Broek: *Eng. Fract. Mech.*, 1973, vol. 5, pp. 55-66.
7. C.Q. Chen and J.F. Knott: *Met. Sci.*, 1981, vol. 15, pp. 357-64.
8. A.K. Vasudevan and R.D. Doherty: *Acta Metall.*, 1987, vol. 35, pp. 1193-219.
9. M. Gräf and E. Hornbogen: *Acta Metall.*, 1977, vol. 25, pp. 877-89.
10. O.E. Alarcon, A.M. Nazan, and W.A. Monteiro: *Mater. Sci. Eng.*, 1991, vol. 138, pp. 275-85.
11. E. Di Russo: *Metall. Sci. Technol.*, 1986, vol. 4, pp. 37-48.
12. R.C. Dorward and D.J. Beerntsen: *Metall. Trans. A*, 1995, vol. 26A, pp. 2481-84.
13. G.M. Ludtka and D.E. Laughlin: *Metall. Trans. A*, 1982, vol. 13A, pp. 411-25.
14. D.S. Thompson and R.E. Zinkham: *Eng. Fract. Mech.*, 1975, vol. 7, pp. 389-409.
15. S.V. Kamat and J.P. Hirth: *Acta Mater.*, 1996, vol. 44, pp. 201-8.
16. J.K. Park and A.J. Ardell: *Metall. Trans. A*, 1983, vol. 14A, pp. 1957-65.
17. D.S. Thompson, B.S. Subramanya, and S.A. Levy: *Metall. Trans.*, 1971, vol. 2, pp. 1149-60.
18. W.M. Garrison, Jr. and N.R. Moody: *J. Phys. Chem. Solids*, 1987, vol. 48, pp. 1035-74.
19. J.D. Embury and E. Nes: *Z. Metallkd.*, 1974, vol. 65, pp. 45-57.
20. K. Welpman, A. Gysler, and G. Lutjering: *Z. Metallkd.*, 1980, vol. 71, pp. 7-14.
21. J.F. Knott: *Met. Sci.*, 1980, vol. 14, pp. 327-36.
22. J.T. Staley: *Mater. Sci. Tech.*, 1987, vol. 3, pp. 923-35.
23. R.J. McElroy and Z.C. Szkopiak: *Int. Met. Rev.*, 1972, vol 17, pp. 175-89.
24. M. Sugamata, C.P. Blankenship, Jr., and E.A. Starke Jr.: *Mater. Sci. Eng.*, 1993, vol. A163, pp. 1-10.
25. A. Deschamps and Y. Brechet: *Mater. Sci. Eng.*, 1998, vol. A251, pp. 200-7.
26. J.-C. Ehrstrom: Pechiney CRV, Voreppe, France, private communication, 1997.
27. T. Kirman: *Metall. Trans.*, vol. 2, pp. 1761-70.
28. I. Sinclair and P.J. Gregson: *Mater. Sci. Forum*, 1997, vol. 242, pp. 175-80.
29. A.M. Gokhale, N.U. Deshpande, D.K. Denzer, and J. Liu: *Metall. Mater. Trans. A*, 1998, vol. 29, pp. 1203-10.